

Broadband Spectral Probing Revealing Ultrafast Photochemical Branching after Ultraviolet Excitation of the Aqueous Phenolate Anion

Xiyi Chen,[†] Delmar S. Larsen,[‡] and Stephen E. Bradforth^{*}

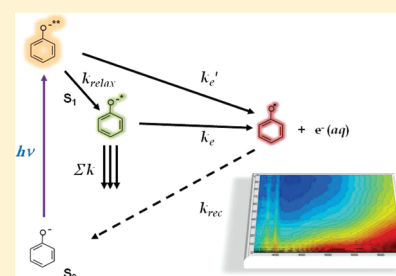
Department of Chemistry, University of Southern California, Los Angeles, California 90089, United States

Ivo H. M. van Stokkum

Department of Biophysics, Faculty of Sciences, Vrije Universiteit, 1081 HV Amsterdam, Netherlands

 Supporting Information

ABSTRACT: Electron photodetachment from the aromatic anion phenolate excited into the $\pi-\pi^*$ singlet excited state (S_1) in aqueous solution is studied with ultrafast transient absorption spectroscopy with a time resolution of better than 50 fs. Broadband transient absorption spectra from 300 to 690 nm are recorded. The transient bands are assigned to the solvated electron, the phenoxyl radical, and the phenolate S_1 excited state, and confirmation of these assignments is achieved using both KNO_3 as electron quencher and time-resolved fluorescence to measure singlet excited state dynamics. The phenolate fluorescence lifetime is found to be short (~ 20 ps) in water, but the fast decay is only in part due to the electron ejection channel from S_1 . Using global target analysis, two electron ejection channels are identified, and we propose that both vibrationally hot S_1 state and the relaxed S_1 state are direct precursors for the solvated electron. Therefore, electron ejection is found just to compete with picosecond time scale vibrational relaxation and electronic radiationless decay channels. This contrasts markedly with <100 fs electron detachment processes for inorganic anions.



1. INTRODUCTION

Phenolate, together with its acidic form phenol, has been used as a prototype for photoinduced electron ejection from low ionization potential aromatic molecules such as indole, aniline, and naphtholate.^{1–5} Structurally all these molecules have electron donor groups, such as $-\text{OH}$, $-\text{O}^-$, $-\text{OR}$, or $-\text{NH}_2$, attached to a conjugated π -ring system.⁶ When photoexcited from their electronic ground state, S_0 , into their first singlet excited state, S_1 , electron ejection is observed to be one of several relaxation channels. Both S_0 and S_1 in the case of phenolate have charge transfer (CT) character, with the lone pair electrons of the donor group partially transferred to the aromatic π -ring.⁷ The CT character can be more pronounced in the excited states, and it has even suggested that when these molecules are excited in aqueous solution, an electron is detached from the aromatic π -ring structure rather than the electron rich donor group itself.⁶ However, there is some recent controversy in the literature as to the energetic ordering of the singlet excited states in molecules such as phenolate,⁷ and explicit consideration of the solvent shifts on all relevant vertical excitation energies or the effect of solvation on the CT character has not yet been made.

Studies of electron photoejection from phenolate and phenol and model chromophores for the deprotonated and protonated form of tyrosine residues in proteins, together with past studies on indole^{8,9} as a model for tryptophan containing proteins, have important biochemical relevance. In particular, the detached

form, the phenoxyl radical, is a good model for the tyrosyl radical, which is implicated as an intermediate in many enzyme reactions.¹⁰ In addition, electron detachment from a phenolate moiety is a reaction channel in the initial photodynamics under femtosecond laser conditions for the photoreceptor chromophore in photoactive yellow protein.¹¹

Although it is widely accepted that for these aromatic molecules in solution, transition into electronically excited valence states leads to ionization,^{1,12–14} it is less clear what the mechanism for the electron ejection is. Much of the early work on these systems speculated on this topic on the basis of measurements of fluorescence and electron yields; the response of these observables to experimental conditions, such as temperature and excitation wavelength; and the change in yields when a foreign species is added into the solution, such as an electron scavenger, a triplet state quencher, or a heavy atom species, which increases intersystem crossing.^{6,15–19}

When nanosecond and picosecond pulsed lasers became available, they were applied to investigation of electron detachment or ionization of these aromatic molecules.^{20–24} These new

Special Issue: Graham R. Fleming Festschrift

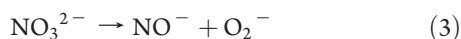
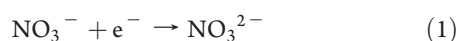
Received: August 21, 2010

Revised: December 9, 2010

Published: January 04, 2011

measurements led to several, and often contradicting, results about electron ejection mechanism. Three originating states for the ejection of an electron have been suggested: (1) a singlet excited state,^{16,17,20,21,24,25} (2) a triplet excited state,^{15,21–23,26} and (3) a charge-transfer-to-solvent (CTTS) state.^{6,18,19} Application of femtosecond transient absorption measurement in this area should allow for unraveling of the early time photoelectron detachment dynamics directly.^{9,27,28} Mialocq et al. obtained transient absorption at 630 nm for aqueous phenolate with a ~ 27 ps resolution and reported “instantaneous” electron ejection.²⁹

The current transient absorption measurements with time resolution of <50 fs are able to considerably better resolve the early time dynamics for electron ejection from phenolate. On the other hand, as has been shown before,^{8,9} transient absorption is sensitive to multiple species, not just the ejected electron, and without knowledge of the spectra of each intermediate, it is difficult to correctly disentangle the deactivation mechanism. With an ability to simultaneously record the full transient absorption in a spectral window across the near-UV and visible range combined with global analysis to process the full data set in a comprehensive way, the dynamics of all involved transient species can be monitored. One of the major techniques in our effort to resolve the entanglement of the absorption of all involved transient species is to use nitrate as an electron quencher that resolves the absorption band of phenoxyl radical from its geminate partner, the solvated electron. Nitrate removes solvated electrons both by diffusive scavenging and by transforming the initially excited state, S_1 , directly into the radical, R, via a “static” electron quenching process.^{30,31} The reactions are shown below:



We find that only by establishing correlations of spectral signatures and their time evolution with and without the addition of quenchers can a full picture be derived of the early time events so that the details of the electron ejection mechanism are finally revealed.

In this work, we report the entire ultrafast transient absorption spectrum from 300 to 690 nm for aqueous phenolate photoexcited at 266 nm with sub-50 fs time resolution. Clear-cut spectral assignment is made possible via an electron quenching experiment and a parallel time-resolved fluorescence measurement. As a result, a detailed electron ejection mechanism is proposed. By modifying the standard approaches to global target analysis so that nonexponential decay processes can be handled, multiple two-dimensional transient absorption data sets are simultaneously fit and cleanly resolved into solvated electrons and phenoxyl radicals, as well as short-lived phenolate S_1 state.

2. EXPERIMENTAL SECTION

A UV pump/broad-band probe transient absorption setup was used in this work to follow the ultrafast dynamics of phenolate electron photodetachment. UV pump pulses were obtained by converting 800 nm laser pulses from a Ti-sapphire regenerative amplifier (Spectra Physics Hurricane, 1 kHz) into 266 nm using a hollow core fiber four-wave mixing scheme.³² The fiber was filled with argon gas, the pressure of which was optimized to 253 Torr for best conversion efficiency into the third harmonic. The 266 nm pulses were then compressed with a prism pair before

they were sent to the sample. The UV pump beam was focused to a diameter of $270 \mu\text{m}$ full width at half-maximum (fwhm), and its pulse energy at the sample was $1.2 \mu\text{J}$. The probe beam was a white light continuum obtained by focusing $2\text{--}3 \mu\text{J}$ of the 800 nm beam into a CaF_2 plate. After going through an optical delay translation stage, the white light beam was brought to a focus (diameter of $\sim 100 \mu\text{m}$) at the sample by a concave reflective aluminum mirror. The probe light was then dispersed by a spectrograph onto a 256 pixel silicon diode array, where wavelength components between 290 and 700 nm, with and without the pump pulse present at the sample, were recorded for each probe pulse and sent to a computer, where the shot-to-shot transient absorption was calculated. Two spectrograph gratings were used to fully cover the 290–700 nm spectrum in two experimental scans. The instrument wavelength resolution is ~ 2.5 nm at best, an estimate based on focusing the probe light to a spot size of $\sim 100 \mu\text{m}$, twice as wide as the pixel size. The optical delay stage was carefully aligned so that the pump/probe overlap deviated less than 3% over the entire 500 ps probe time window. The sample was delivered using a wire-guided gravity-driven (WGGD) flow jet of $\sim 80 \mu\text{m}$ thickness.³³ The instrument response function (IRF) at 450 nm was measured as ~ 47 fs, and was comparable at other wavelengths.

Time-resolved fluorescence measurement was performed with a time-correlated single photon counting apparatus (TCSPC) described in ref 34. The 266 nm excitation wavelength was generated by frequency-doubling the visible output of an optical parametric amplifier (OPA), which is pumped by a 200 kHz Ti:Sa amplifier system (Coherent Mira/RegA 9050). The excitation pulses had a bandwidth of ~ 3.2 nm. Fluorescence emission at 330 nm was collected perpendicular to the excitation beam and sent to a monochromator with a 0.6 mm input slit that corresponds to a bandpass of 2 nm. The photons were detected by a Hamamatsu RU3809 PMT operating at -3.0 kV. The signal was then analyzed on a computer equipped with a Becker and Hickl SPC-630 photon counting board. A small fraction of the visible beam was monitored with a fast photodiode for timing purposes. Spontaneous water Raman scattering from the solution at 292 nm was recorded to characterize the IRF (25 ps) of the TCSPC setup for the 266 nm excitation wavelength.

Phenol (99.5%) purchased from Avocado Research Chemicals Ltd. was dissolved in deaerated water (deionized water from Sparklets) to make all solutions used in this paper. NaOH (0.1 M) (Mallinckrodt, 98.7%) was added to the solutions so that the deprotonated form dominates the total phenol/phenolate concentration ($>99\%$). The concentration of phenolate was adjusted for fluorescence-based measurements so that the sample optical density at the excitation wavelength was 0.1. For the transient absorption measurements, a much higher concentration (90–100 mM) was used to suppress the transient solvated electron signal from water and hydroxide to less than 1%. For the electron quenching study using KNO_3 (Mallinckrodt, 99.72%), two solutions were made by adding KNO_3 to the 90 mM phenolate/0.1 M NaOH solution to achieve 0.2 and 0.5 M in nitrate, respectively, and another phenol/NaOH solution was prepared to be 0.2 M in NaCl to be compared with the 0.2 M KNO_3 solution at the same ionic strength.

3. RESULTS

3.1. Steady State Absorption and Fluorescence Spectroscopy.

At room temperature, phenolate has its lowest singlet absorption

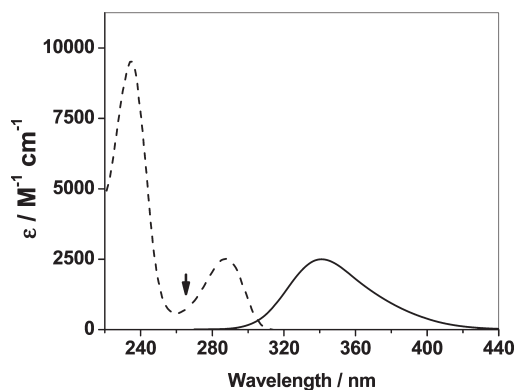


Figure 1. Steady-state absorption (dashed) and fluorescence (solid line) spectra for phenolate at pH 13. The water Raman scattering signal has been removed in the fluorescence spectrum by direct subtraction. The intensity of the fluorescence spectrum has been scaled for visual presentation. The arrow indicates the excitation wavelength for the fluorescence and transient absorption described in this work.

band peaking at 287 nm. (Figure 1) The center of the second resolved band is at 234 nm, which has been assigned to S_2 .⁶ Both transitions are valence $\pi-\pi^*$ transitions.¹ No CTTS character is observed in these transitions.¹ The static fluorescence emission spectrum for aqueous phenolate solution at room temperature is also shown in Figure 1. The emission spectrum is one broad band that peaks at 340 nm, and it crosses the absorption spectrum at 305 nm when it is rescaled so that its band magnitude matches the S_1 absorption band. The fluorescence emission from phenolate is very weak, and therefore, water Raman scattering shows up as a sharp band at 293 nm in the emission spectrum; this has been subtracted from Figure 1.

3.2. Time-Resolved Fluorescence. Figure 2 shows the fluorescence time-resolved profile when 266 nm is used as the incident light and fluorescence emission at 330 nm is collected. It can be seen that the fluorescence emission decays very fast, with a time constant comparable to the 25 ps IRF width. A careful estimate of the fluorescence decay constant can be achieved by comparing the time-resolved emission with simulations involving convolution of the IRF with a single exponential function. Figure 2 indicates that a fluorescence decay constant of 22 ± 2 ps can be recovered at 266 nm excitation wavelength.

3.3. Time-Resolved Transient Absorption. Pump-induced broad-band transient absorption measurement provides rich, two-dimensional data that records spectra of the excited system at different time delays. The contour plot in Figure 3 displays a full transient absorption data set in the range of 360–640 nm when 100 mM aqueous phenolate is excited at 266 nm. The features of the transient spectra and their kinetics can be better revealed by the spectral and time slices. Figure 4a shows transient absorption spectral slices for a 90 mM phenolate solution excited at 266 nm at a series of time delays, from 2.5 to 500 ps, focusing on the 320–560 nm probe wavelength range. Figure 4c displays the temporal variation of the transient absorption at three selected wavelengths when they are scaled to match at long times. It can be seen that at all wavelengths, the transient absorption appears instantaneously after photoexcitation and keeps increasing up to a maximum at 3–5 ps, depending on the probe wavelength, and then decreases until ~ 100 ps, when the profiles start to level off. Figure 4c also indicates that the dynamics starting from ~ 40 ps probed at different wavelengths are identical. This can also be

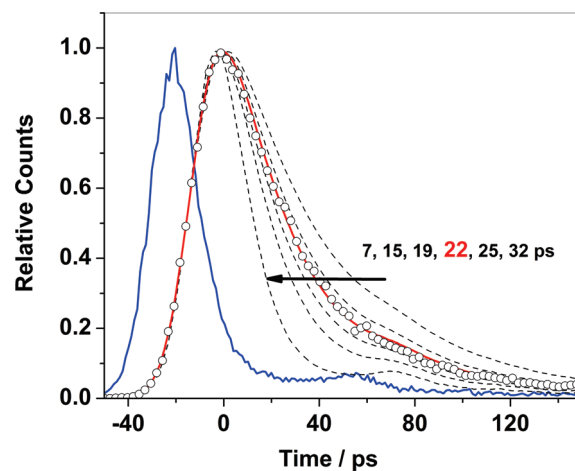


Figure 2. Picosecond time-resolved fluorescence data for 5 mM phenolate at pH 13. Experimental fluorescence data (open circles); the blue line is the instrument response, IRF, which for clarity has been displaced by -20 ps. Black dashed lines are the convolution of the IRF with varying time constant single exponential decay functions (values left to right shown above arrow). The red solid curve represents the best-fit 22 ps decay constant.

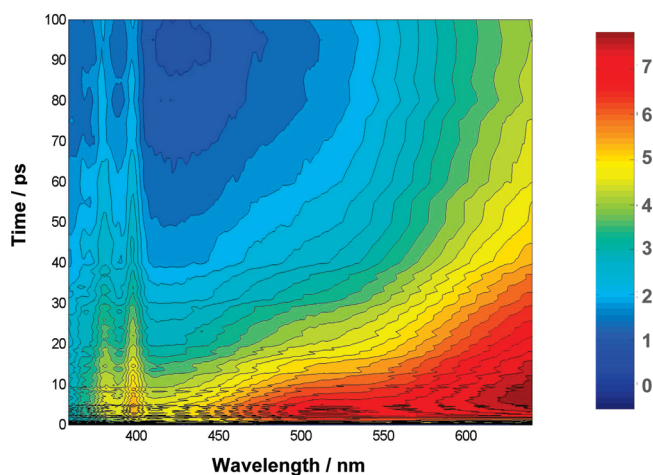


Figure 3. Contour plot of the full 2D transient absorption data set (visible grating) of 100 mM phenolate (pH = 13) solution at 266 nm. A color bar (in units of mOD) is shown to the right.

seen in Figure 4a, where the shape of the spectra at delays >40 ps does not change.

There are two dominant features present in all the spectra shown in Figure 4a. The first is the broad absorption band appearing in the red, and the second is a double-peak structure between 340 and 400 nm. The absorption spectrum of equilibrated solvated electron in water is also included for comparison, and it matches up well with the 500 ps transient absorption to the red of 450 nm. When 0.5 M nitrate anion is added to the solution, the broad band in the red edge is suppressed and is completely eliminated by 500 ps (Figure 4b) while the double-peak structure in the blue survives. It is very interesting to notice, after a careful examination of Figure 4a and b, that this second structure in the blue is actually enhanced when nitrate anion is present. At 394 nm, the most intense peak in the structured band, the transient absorption is 0.85 mOD at 500 ps in the nitrate solution, but for the solution

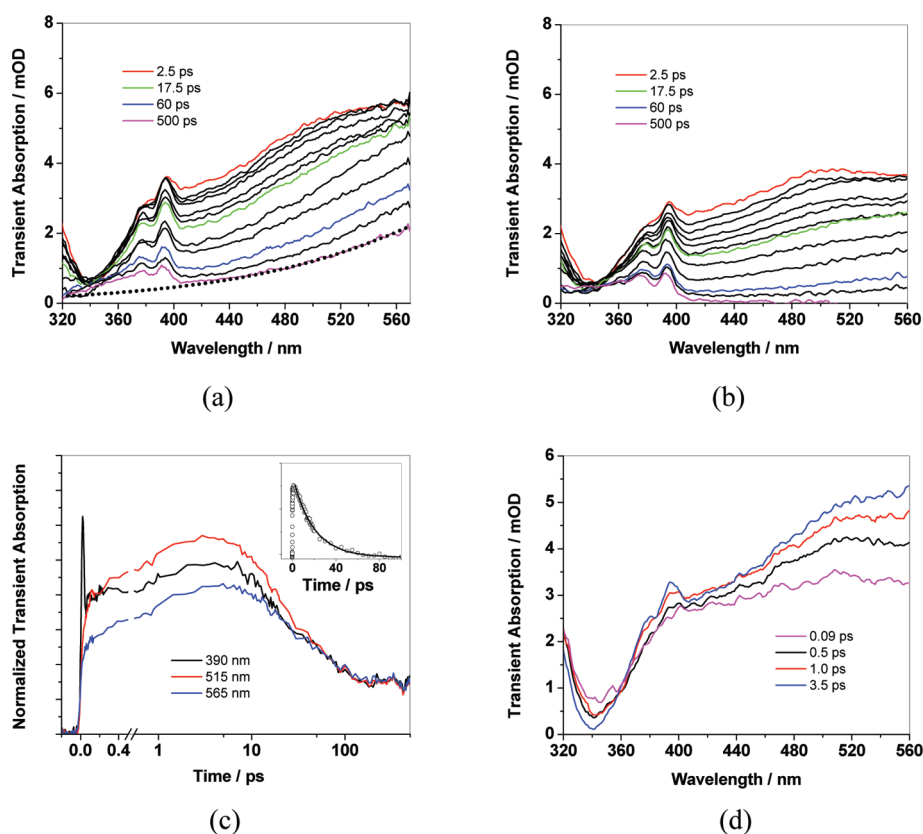


Figure 4. Photoinduced transient absorption of 90 mM phenolate solution at pH 13. Excitation wavelength used is 266 nm. (a) Spectral slices at a series of delay times. Transient spectra at representative delay times are color-coded. The equilibrium solvated electron absorption spectrum (dotted) is included for comparison.⁵⁰ (b) Spectral slices for the phenolate solution when 0.5 M nitrate is added. The delay times plotted are the same as in panel a. Pump laser intensity and sample jet thickness variation are corrected to make direct comparison with panel a. (c) Temporal profiles recorded at 390, 515, and 565 nm. Transient absorption is normalized to 500 ps. Note the time axis is linear until 0.5 ps and logarithmic thereafter. The zero delay spike for the 390 nm profile is due to simultaneous absorption of one pump and one probe photon by the solvent. From this feature, an IRF of <50 fs (fwhm) can be estimated at this probe wavelength. (Inset) Transient absorption difference (circles) between slices at 565 and 515 nm. See text for details. The solid line is an exponential decay function with a time constant of 19 ps. (d) Transient spectra, as in panel a, but at early delays.

without nitrate, the same peak is 0.50 mOD above the baseline formed by the solvated electron spectrum profile in this spectral region.

On closer inspection of Figure 4a, it can be seen that at times earlier than ~ 40 ps, there are two other spectral features that are absent at longer times. Most obviously, between 460 and 560 nm, a modest additional spectral component is superimposed on top of the broad absorption band peaking in the red. As a result, the spectral profile curvature changes within this time window. The other structure is a “negative” absorption component, centering around 340 nm, forming a spectral “valley”. These two bands share similar decay dynamics and seem to share a common population source. To show the early time dynamics, four transient absorption spectra within the first 3.5 ps are plotted in Figure 4d. It is observed that the transient absorption appears instantaneously (within 90 fs) after photoexcitation across the whole spectral range, and the shape of the spectrum evolves quickly. At 90 fs, the blue double-peaked absorption structure is not distinct, and it becomes well-developed at 3.5 ps. In this time window, the broad absorption band in the red edge increases in its magnitude while the 340 nm spectral “valley” deepens. The center of the negative component continuously shifts to the blue by ~ 4 nm (Figure 4d), and then stays at 340 nm until it has completely disappeared at ~ 100 ps (Figure 4a).

4. DISCUSSION

4.1. Transient Absorption Assignment. We observe that upon excitation of phenolate, transient absorption appears immediately across the whole UV/vis range (Figure 3). The rise of the transient absorption signal displays a biphasic behavior. It rises instantaneously within our time resolution of better than 100 fs and then keeps increasing at a slower rate to a maximum within the first several picoseconds before it starts to decrease (Figure 4c). The previous section clearly showed that solvated electrons are produced (Figure 4a), but it also revealed that the transient absorption spectrum is not solely due to solvated electron. The swift evolution of the spectrum shape at early times is a sign that other transient species are also created and they undergo fast dynamics. For any meaningful dynamic information to be retrieved from time-resolved transient absorption, the spectrum has to be assigned first.

Several transient species, whose identities and temporal behaviors are not initially known, may form after photoexcitation. The solvated electron has a very characteristic absorption spectrum peaking at 720 nm, so it is straightforward to assign the broad transient absorption on the red end of our probing range to the solvated electron. The static solvated electron absorption spectrum matches well with the $t = 500$ ps transient spectrum at

wavelengths longer than 450 nm (Figure 4a). This indicates that at 500 ps (in fact, at any time longer than ~ 40 ps), the solvated electron is the only transient absorbing in this wavelength range, since the shape of the transient spectrum remains unchanged thereafter. Excitation intensity studies (not shown) establish that the transient absorption in the red at long times scales linearly with pulse energy with a zero intercept, and thus, electrons are produced by absorption of a single pump photon.

The 500 ps transient absorption deviates from the electron spectrum only at bluer wavelengths, particularly in the 350–400 nm range, where structured absorption is observed. We assign this second band to phenoxyl radical absorption, since its dynamics exhibit behavior identical to the solvated electron at longer times (Figure 4c). This is strongly supported by the phenoxyl radical absorption measured in argon matrix at 7 K, which shows an electronic band peaking at 396 nm with similar vibronic structure.³⁵ The nitrate electron scavenging experiment confirms this assignment for the electron and the radical (Figure 4a and b). Without nitrate, the electron and phenoxyl radical absorption decay together as a result of geminate recombination. When the nitrate is present, the absorption beyond 510 nm decreases to baseline long before 500 ps because all electron population is removed by nitrate scavenging. The effect of the scavenging reaction on the radical dynamics is to increase radical production, as indicated by the transient absorption at 394 nm; more radical survives due to the removal of its recombination partner. Similar spectral structure around 400 nm in the transient absorption is also observed after *p*-cresolate and tyrosine are photoexcited in water and the two peaks are explained as vibrational bands of the radical electronic absorption.^{36,37}

We are left with assigning the two features at ~ 500 and ~ 340 nm, respectively. Both features disappear completely before 40 ps, as indicated by Figure 4a, c. The differences between the transient absorption temporal profiles within the first 40 ps in Figure 4c reflect the dynamics of a broad feature that is superimposed on the electron/radical absorption. The difference between transient absorption traces at 515 and 565 nm (curves in Figure 4c) is plotted in the inset of Figure 4c. Because the time-resolved absorption profiles in Figure 4c were normalized at 500 ps, the trace in the inset effectively no longer has any contribution from the long-lived solvated electron or the phenoxyl radical, except possibly in the first ~ 2 ps when the electron absorption spectrum may be time-dependent due to solvation.³⁸ The trace in the inset displays a fast rise, and from 2 ps onward, the decay can be fitted with an exponential function with a decay time constant of 19 ± 2 ps. Now the question becomes, what species can have such a lifetime to account for this transient absorption component?

Let us consider possible candidates. When phenolate is first photoexcited at time zero, the vertically populated state is the singlet excited state, S_1 . Theoretically, a triplet excited state, T_1 , could also be formed from the S_1 state via intersystem crossing (ISC). Therefore, in addition to the solvated electron and the phenoxyl radical, phenolate in its S_1 state and T_1 state may also contribute to the absorption in the green. Both states of this type of aromatic molecules have, in fact, been suggested to be the direct parent for the solvated electron and radical.^{15–17,20–26} However, the excited state absorption (ESA) spectral bands have not been previously reported for phenolate S_1 or T_1 , although triplet state absorption of phenol is observed at wavelengths shorter than 500 nm.¹⁵ The phenol triplet state lifetime is 3.3 μ s, typical of an aromatic triplet state at room temperature. This is 4 orders of magnitude longer than the decay time of the 515 nm

transient absorption feature. It is unlikely that for phenolate, the triplet lifetime has decreased so dramatically. The best candidate to explain the transient absorption around 515 nm is the S_1 state. Indeed, our time-resolved fluorescence measurement demonstrates that the phenolate S_1 lifetime is extremely short, and this is consistent with the significantly reduced fluorescence yield in the anionic form (at room temperature in water, phenolate and phenol fluorescence quantum yields at 254 nm are 0.007 and 0.12 respectively,⁶ and phenol has an S_1 lifetime 100 times longer in water, ~ 2 ns).¹⁵ The fluorescence lifetime recovered here, 22 ± 2 ps (Figure 2), agrees well quantitatively with the decay time constant of the transient absorption feature at 515 nm (Figure 4c inset). The “negative” absorption at 340 nm can be readily attributed to stimulated emission (SE) from the S_1 state because this spectral band overlaps well the static fluorescence emission (Figure 1), and the time scale for its disappearance also matches the fluorescence lifetime.

In summary, the photoinduced transient absorption can be attributed to the solvated electron and the phenoxyl radical across the whole time window, as well as absorption and stimulated emission from the S_1 state at times less than ~ 40 ps. No transient absorption assignable to the triplet state is required. At early time, the spectra of the three assigned transient species overlap, but at longer time, when S_1 has decayed, the spectra of the solvated electron and the radical can be completely resolved using nitrate as the electron scavenger.

4.2. Electron Ejection Mechanism. It has long been established that an electron can be ejected after phenolate is excited into its S_1 state in aqueous solution.¹ The geminate partner, the phenoxyl radical, is also created at the same time. The geminate pair is not necessarily tightly bound: the radicals are produced at a range of separations (up to a few nanometers), depending on the mechanism for the electron ejection, and are subsequently free to diffuse, either recombining or escaping each other.^{39–41} The radicals are considered geminate in the sense that they originate from the same parent. What is not certain is how fast the initial ejection of an electron happens and which state is responsible. A very simple instantaneous electron ejection picture was proposed when Mialocq found that transient absorption at 630 nm rises entirely within their 27 ps pulse duration when phenolate was photoexcited at 265 nm.²⁹ He assigned the photoinduced transient signal solely to solvated electrons, on the basis of electron scavenging experiments.

With our improved time resolution and complete spectral information across the UV/vis region, we have demonstrated that the electron ejection is more complex. First, the distinct phenoxyl radical absorption structure around 390 nm is absent at time zero. The vibrationally structured band grows in within the first ~ 3 ps and is not appreciably developed as late as 1 ps (Figure 4d). This means that the solvated electron as the geminate partner of the phenoxyl radical is not created right after photoexcitation. In contrast, for example, photodetachment of $\text{Fe}(\text{CN})_6^{4-}$ leads to observation of detached parent within 100 fs, which indeed indicates instantaneous electron ejection, at least on currently measurable time scales.⁴²

Second, the discussion in the preceding section establishes that the transient species responsible for the instantaneous transient absorption at longer wavelengths in Figure 4a is the “vertical” S_1 excited state. We believe that the instantaneous transient absorption component recorded at 630 nm by Mialocq et al. can be assigned at least in part to the S_1 ESA and electron absorption contributes at longer times.

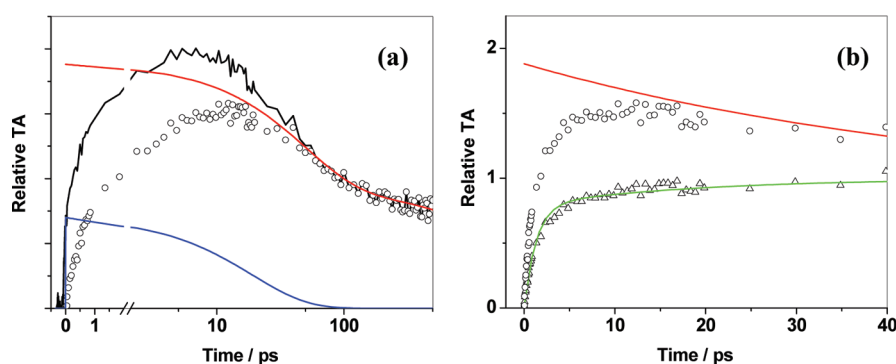


Figure 5. (a) Temporal profile of the transient absorption (black line) of 90 mM phenolate solution (pH = 13) at 650 nm, $\lambda_{\text{ex}} = 266$ nm. This signal is deconstructed into (blue line) the S_1 contribution, with the remainder (circles) representing the solvated electron contribution. In addition, the red line is a biexponential decay to fit to the longer delay recombination behavior in the solvated electron signal (circles, see text). Note that the time axis is linear until 2 ps, and logarithmic thereafter. (b) To extract the electron appearance kinetics (triangles), the first 40 ps of the electron transient signal (circles) is ratioed to the fitted geminate recombination function (red line). The electron appearance curve (triangles) is shown with a biexponentially rising fit (green line).

Since the S_1 dynamics is already known to be characterized by a single exponential 22 ± 2 ps decay, we can remove the S_1 contribution completely from the transient absorption data so that the electron and radical dynamics can then be cleanly revealed. The 650 nm probe transient absorption is used to show this subtraction procedure in Figure 5a. The blue line is the 22 ps decay representing the S_1 dynamics, and its zero time magnitude is set to match the instantaneous component of the transient absorption. The transient absorption after the S_1 signal is subtracted is shown as open circles. At this wavelength, the phenoxyl radical does not absorb (Figure 4b), and the circles in the plots of Figure 5 therefore represent the transient absorption from solvated electrons alone.³¹ The electron transient absorption temporal profile at 650 nm (circles) starts to build up from zero upon photoexcitation and increases until it reaches its maximum at ~ 13 ps before it undergoes a decrease that leads to a loss of $\sim 50\%$ at 500 ps. This clearly shows a qualitatively electron ejection dynamics different from ref 29 in that electron ejection of phenolate is not instantaneous.

Although the precise details of which state is responsible for electron ejection still requires further analysis to unravel (see below), the decay of the electron population can be explained in terms of geminate recombination between the electron and radical. This topic has been discussed in detail in the literature, and the reader is referred to refs 39 and 41 for details. The full analysis of the geminate recombination dynamics will be given in a separate publication. Here, it is sufficient to use a biexponential function to describe the complex nonexponential decay behavior³¹ associated with the pair recombination⁴⁴ by fitting the transient absorption temporal profile starting from 20 ps, when the effect of the formation and thermalization dynamics should be small. The biexponential fit thus obtained is

$$0.51e^{-t/50\text{ps}} + 0.49e^{-t/2900\text{ps}} \quad (4)$$

and is shown in Figure 5 as the red line. The early time geminate recombination is estimated by extrapolating the biexponential function to time zero, a choice that assumes that there is no rapid recombination from any geminate contact pairs formed.³⁹

It is then useful to extract the appearance dynamics of the electron. The entire effect of geminate recombination can be removed by computing the ratio of the electron signal (circles) to the geminate recombination biexponential fit (Figure 5b).

The resulting trace (triangles) is now used to cleanly estimate the time scales for electron ejection and trapping. This step-by-step approach provides a framework for the more thorough global analysis given in Section 4.3.

The electron transient absorption obtained in Figure 5b above can be approximately fitted with a ~ 4 ps exponential growth function but is better described with two rising exponential components. According to an argument of Goldschmidt et al., the rise time of electron population should match the lifetime of its precursor.⁴⁵ The rise time of solvated electron transient absorption is not decided by the electron ejection rate, but rather, is directly correlated with the total depopulation rate of its precursor. Thus, the precursor that generates the solvated electron should have a lifetime of ~ 4 ps. This is supportive for the suggestion that the S_1 state is the origin of the solvated electron, in light of the fact that the S_1 state has a short lifetime. However, if electron ejection takes place only from the S_1 state of the phenolate ion, the rise time of electron transient absorption should match the fluorescence lifetime, which is 22 ± 2 ps (Figure 2). This is still longer than the ~ 4 ps rise time of the solvated electron. Either there is a precursor whose lifetime is shorter than the phenolate fluorescence lifetime or there is more than one precursor, whose average lifetime meets the requirement. With the better biexponential fit of the rise of the electron population in mind, we propose that solvated electrons have two precursors (global analysis below confirms this proposal). Further, we assign the precursor with the longer lifetime to the 22 ps S_1 state. The other precursor lifetime must be shorter than 4 ps, and by fitting the electron rise shown in Figure 5b with a biexponential growth while constraining the longer precursor lifetime to be 22 ps, we obtain

$$0.81\left(1 - e^{-t/1.4\text{ps}}\right) + 0.19\left(1 - e^{-t/22\text{ps}}\right) \quad (5)$$

From the above expression, the lifetime of the earlier precursor (contributing 81% of the total electron population) is given as 1.4 ps. Two candidates can be proposed on the basis of the short lifetime of the precursor for fast electron ejection: a vibrationally unrelaxed S_1 state or a S_1 state prior to solvation dynamics. At this point, we do not distinguish these two possibilities and will discuss the exact nature of this precursor in Section 4.3, below. Because they are both unrelaxed states, we call this short lifetime

singlet state, S'_1 . The relaxed singlet excited state with the 22 ps lifetime we call S_1 .

We now have elaborated a minimal and physically reasonable description for the population dynamics that can model the transient absorption data, and a target kinetic scheme is proposed as a result (Figure 6a). The model goes as follows: after photoexcitation from S_0 , the unrelaxed S'_1 is produced instantaneously. From S'_1 , an electron together with the geminate phenoxyl radical, R, is generated with a rate constant of k'_e , while S'_1 may also relax to S_1 at a rate of k_{relax} . The relaxed S_1 may undergo electron ejection, as well, in addition to the other regular deactivation processes such as IC, ISC, and radiative decay. k_e is used as the electron ejection rate from S_1 , and the other S_1 deactivation rates are summed as Σk . All of the processes so far mentioned are first-order. The final step is that the electron and radical, produced via the above two channels, can then recombine diffusively to form the ground state S_0 , but they may also escape each other.²⁵ k_{rec} is not a first-order decay constant.

4.3. Global and Target Analysis. The two-dimensional, pump-induced transient absorption data obtained with the broad-band probe method (Figure 3) provides much richer spectral and dynamics information than has been analyzed thus far. To fully explore the 2D data, global and target analysis are used to describe all data with the help of a target model containing meaningful physicochemical parameters.^{46,47} It is a very useful tool for a system with multiple absorbing species within the experimental spectral window. Each species has a (time-independent) spectrum associated with it, which is called species associated difference spectrum (SADS).

The transient absorbance for a system with n transient species, $TA(t, \lambda)$ at a given probe wavelength λ and delay time t is given by

$$TA(t, \lambda) = \sum_{j=1}^n c_j(t) \varepsilon_j(\lambda) \quad (6)$$

$c_j(t)$ is the concentration of the j th transient species at time t ; and $\varepsilon_j(\lambda)$ is its SADS. Equation 6 provides a way to resolve the temporal and the spectral information from the 2D data, and the dynamics of the system are now solely described by the concentration of all species, $c_j(t)$. These are not independent, but correlated according to a connectivity scheme, such as Figure 6a. In this scheme, boxes that describe the species are called compartments. The species concentration variation can be described by

$$\frac{dc_i(t)}{dt} = \sum_{j=1}^n k_{ij} c_j(t) \quad (7)$$

where k_{ij} is the rate constant for the j th species transferring to the i th species and k_{ii} corresponds to the rate of concentration loss from the system of the i th species from a process that is not connected to any other named compartment. For example, according to the notation used in Figure 6a, k_{31} corresponds to the electron ejection rate for the unrelaxed S'_1 state k'_e , and k_{22} is the S_1 deactivation rate Σk .

When we start trying to apply the target analysis to the phenolate detachment data, we encounter two problems. The first is that equation set 7 assumes that all the reactions involved are of first-order, which means that the decay dynamics of each of the species can be described by a single exponential function. However, the geminate recombination process is a bimolecular reaction under inhomogeneous spatial conditions and cannot be described as pseudo-first-order.⁴⁸ This obviously does not meet the requirement of the global analysis scheme. Second, in Figure 6a,

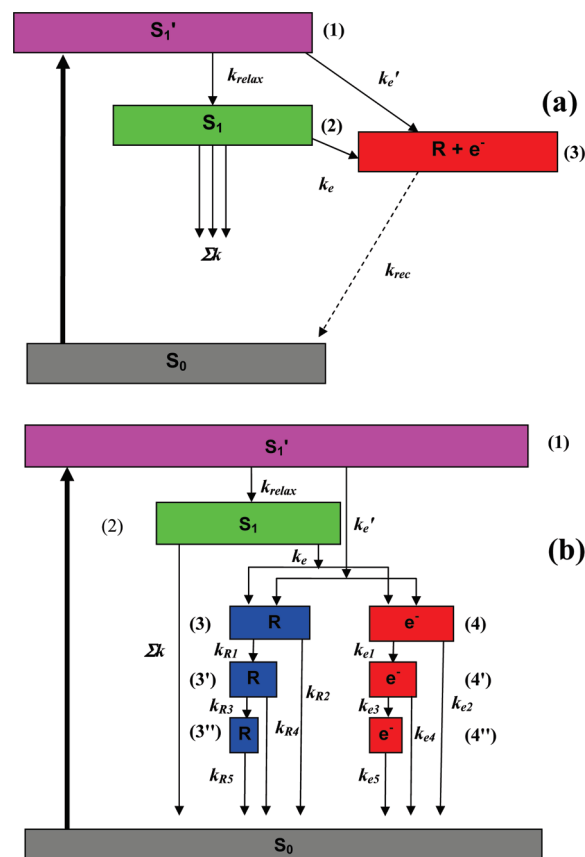


Figure 6. Kinetic scheme for electron ejection. The compartments represent the various transient species in the system color-coded denoting the unique spectral characteristic of the transient species. S_0 is the ground state, S'_1 and S_1 are the excited state before and after relaxation; R is the phenoxyl radical; e^- is the solvated electron. The numbers refer to the species number in eq 6 and 7. k_{relax} is S_1 relaxation; k'_e is for electron ejection from S'_1 ; k_e is for electron ejection from S_1 . Σk is the sum of the deactivation rate constants other than k_e . (a) Single wavelength analysis. k_{rec} represents the geminate recombination process (dashed arrow), which is not treated as a first-order process; see text. (b) Model used to allow description of geminate recombination within a global analysis scheme. Now k_{e1} , k_{e2} , k_{e3} , k_{e4} , k_{e5} and k_{R1} , k_{R2} , k_{R3} , k_{R4} , and k_{R5} are the decay rates for the multiple electron and radical compartments, respectively; see text. Note that in panel b, the multiple electron and radical compartments are coded with the same colors, respectively, indicating that these compartments are not distinguishable spectroscopically.

one shared compartment is used for both the phenoxyl radical and the solvated electron, on the basis of the consideration of their identical population dynamics. However, this is no longer true when KNO_3 is added to quench the electron, separating it from its geminate partner. As observed in Figure 4, the effects of KNO_3 to the electron and to the phenoxyl radical are complementary: the electron quencher removes the electron population and increases the radical population. The Supporting Information gives the mathematical treatment of the quenching effect to a system undergoing geminate recombination. In short, the quenching effect to the electron dynamics can quite simply be described by two factors added to the regular geminate recombination population profile $\Omega(t)$, a constant factor, $1 - \eta$, to account for the static quenching³⁰ and an exponential decay

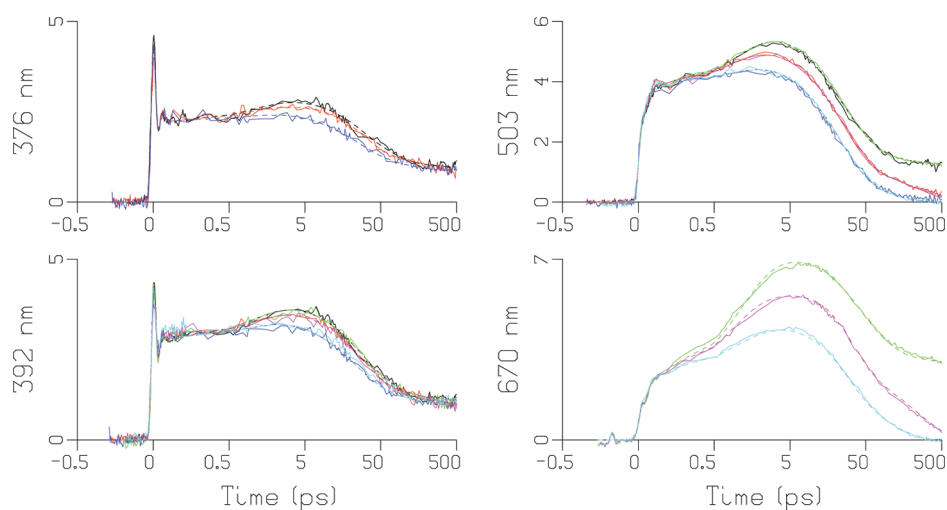


Figure 7. Representative transient absorption traces and their fits (dashed lines) resulting from global target analysis (with three different quencher concentrations) using the kinetic scheme from Figure 6b. Probe wavelength indicated as ordinate label; the transient absorption unit throughout is mOD. Note that the time axis is linear until 0.5 ps and logarithmic thereafter. Key: black and green, 0 M nitrate added; red and magenta, 0.2 M; blue and cyan, 0.5 M. Note that with probes below 460 nm, a coherent artifact is present at zero delay arising from two-photon absorption of the solvent. This was modeled as a sequence of three short-lived components (≈ 10 fs). Further explanation is provided in the caption of Figure S2. Rate constants obtained from the fit are shown in Table S1.

factor, $\exp(-k_q[Q]t)$, to account for the diffusive bimolecular quenching that can be treated as pseudo-first-order.^{29,40}

The effect of the electron quencher on the phenoxyl radical dynamics is more complicated because the nature of $\Omega(t)$ usually cannot be described by an analytical expression, and numerical integration is needed. However, if $\Omega(t)$ is simplified as a biexponential function, as has been assumed so far, then both the electron and radical dynamics can be derived analytically, which is also shown in the Supporting Information. Figure S1 clearly indicates that with electron quencher present, the radical and the electron follow different dynamics. To reflect the uniqueness of the system under study, we modified the kinetic scheme as shown in Figure 6b. The radical and the electron are now treated separately so that they can execute different dynamics. In addition, for both the radical and electron populations, three compartments with identical SADS are used. This is introduced to give enough freedom so that the geminate recombination and the electron quenching kinetics can be reproduced. For instance, the electron now has three decay components with rate constants of $(k_{e1} + k_{e2})$, $(k_{e3} + k_{e4})$ and k_{e5} , respectively, with two components for the biphasic geminate recombination and one for the fast static quenching. The target analysis simultaneously fits data sets with three different quencher concentrations over the full UV/vis spectral range. However, the full constraint implied by the mathematical description of the electron quenching dynamics in the supplement is hard to fully implement, and we verify in the Supporting Information that a satisfactory quenching description is achieved by comparison with the derived electron and radical survival possibilities, $[e^-](t)$ and $[R](t)$.

Rate constants estimated earlier from the single wavelength treatment are used as initial estimates for the global analysis. In addition to the kinetic scheme, three spectral constraints are used in the target analysis: the radical SADS is equal to zero for wavelengths longer than 500 nm and the S'_1 and S_1 SADS were forced to be identical for $\lambda > 660$ nm. Below 328 nm, the shapes of the solvated electron and radical SADS were equated, since the decreased signal-to-noise ratio in this spectral range precluded

Table 1. Rate Constants Estimated from Global Target Analysis

$k_{\text{relax}}/\text{ps}^{-1}$	k'_e/ps^{-1}	k_e/ps^{-1}	$\Sigma k/\text{ps}^{-1}$
0.68	0.19	0.027	0.027

full resolution of both SADS independently. These constraints aided in the parameter estimation and resulted in meaningful estimated parameters (SADS and rate constants). The parameters of this target model are the SADS and the rate constants k_{ij} . These are estimated from the fit of eq 6 to the experimental data. The target analysis simultaneously fits two-dimensional data sets with three different quencher concentrations over two wavelength ranges (corresponding to two different diffraction gratings) using five additional scaling parameters to allow for small variations in the laser intensity between these different data sets. Representative traces and their fits are depicted in Figure 7.

The estimated values from the global target analysis for selected rate constants are collated in Table 1; the full list of rate constants is given in Table S1. Table S2 provides the lifetimes for each compartment and, for the electron and radical, the amplitudes associated with these species' multiexponential decay. The lifetime of the S_1 state estimated from the global target analysis is 18.5 ps. This is quite close to the fluorescence lifetime of 22 ps from the TCSPC measurement with its error bar in mind (Figure 2). This is also the rise time for the slow electron ejection. The S'_1 lifetime, which determines the rise time for the fast electron ejection, is estimated to be 1.15 ps. From the global target analysis, estimated SADS for each species are shown in Figure 8a, and the time-dependent populations for each species (for the case of no electron quencher) are plotted in Figure 8b. Because the first recombination lifetime (τ_{R1} or τ_{e1} in Table S2) is faster than the S_1 lifetime (18.3 ps), this inverted kinetics leads to relatively low peak concentrations for e^- and R.

We find that our global target analysis has satisfactorily handled the electron quenching dynamics (Figure 9). Nitrate is known as a diffusive electron quencher^{29,49} as well as a static

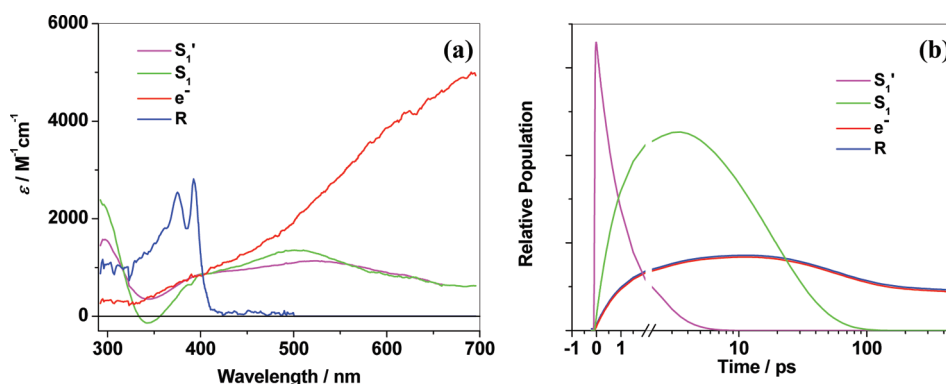


Figure 8. Absorption spectra (a) and relative populations (b) of the solvated electron (red, magnitude rescaled by a factor of 1/3), the phenoxyl radical (blue), the relaxed S_1 state (green), and the unrelaxed S_1' state (magenta) estimated from global target analysis of the 2-dimensional transient absorption data using the kinetic scheme from Figure 6b. In panel b, the populations of the transient species are shown for the solution without KNO_3 . The radical dynamics is identical to the electron, and its trace is vertically translated slightly so that it is visible.

one.³⁰ By using it here, we have demonstrated an important approach not only to verify the electron signal but also to completely separate the absorption spectrum of the phenoxyl radical from that of the electron. The electron population profiles recovered from the global analysis of the 0, 0.2, and 0.5 M KNO_3 phenolate solutions are displayed in Figure 9, and this figure confirms that the electron quenching kinetics denoted by eq 5 in the Supporting Information are fully satisfied. The bimolecular scavenging rate constant of nitrate k_q is estimated as $0.020 \text{ ps}^{-1} \text{ M}^{-1}$. The same value was obtained for the electron quenching rate constant of NaNO_3 by Aldrich et al.,⁴⁹ over the NaNO_3 concentration range of 0.1–0.75 M, and it is also quite consistent with the value measured by Mialocq et al. for 0.5 M quencher concentration.²⁹ These observations give us confidence in the performance of the global target analysis and strongly support the mechanism we propose for the electron detachment from phenolate. From the scaling factor of the electron profiles in Figure 9, the static quenching factor η , of eq 5 in the Supporting Information can also be extracted, and it is found to be 0.21 and 0.45 for the 0.2 and 0.5 M KNO_3 solutions, respectively.

Let us now examine the recovered spectra of the transient species (Figure 8a) more carefully. The solvated electron absorption spectrum profile reproduces the literature spectrum⁵⁰ very well, making the global analysis and the target scheme very convincing. Via simultaneously fitting three data sets at different [quencher] the radical spectrum is completely resolved from the electron spectrum. The phenoxyl radical electronic spectrum was recorded across the whole UV–vis–IR region by Radziszewski et al. using a polarization spectroscopy technique in an argon matrix at 7 K.³⁵ A pronounced band between 380 and 400 nm is observed with Franck–Condon profile similar to the SADS in Figure 8a. A similar phenoxyl radical double-peak absorption band around 400 nm was observed by Ichino et al. after photodetachment of aqueous *p*-cresolate³⁶ and by Feitelson et al. from tyrosine photodetachment in their microsecond flash photolysis study.³⁷ Even though the medium and the experimental conditions are very different, the radical absorption spectrum for phenoxyl estimated in aqueous solution matches the matrix study surprisingly well in three additional aspects: First, the vibrational peaks of the recovered absorption band at 392 and 376 nm show up at 396 and 383 nm in the matrix study. Second, the maximum extinction coefficient of the radical absorption band is recovered as $3155 \text{ M}^{-1} \text{ cm}^{-1}$ from the global analysis in our study, and it is very

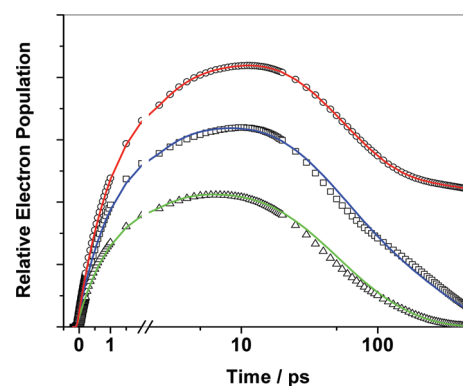


Figure 9. Time-dependent electron populations recovered from the simultaneous global analysis of three data sets different with varying concentration of NO_3^- electron quencher: (circles) 0, (squares) 0.2, and (triangles) 0.5 M NO_3^- . The variation in electron population extracted in each case from the global model is tested against the correct physical functional form on the basis of bimolecular diffusive quenching (lines). The population profile in the absence of quencher defines the unperturbed electron population function $P(t)$ (red line), and the blue and green lines are simply $(1 - 0.21) P(t) e^{-0.02 \times 0.2 \times t}$ and $(1 - 0.45) P(t) e^{-0.02 \times 0.5 \times t}$, respectively. Note that the time axis is linear until 2 ps, and logarithmic thereafter.

close to the estimated value, $3600 \text{ M}^{-1} \text{ cm}^{-1}$, in the matrix study.³⁵ Third, the matrix study recorded a very weak absorption spread over many vibrational states, peaking at 606 nm, whose extinction coefficient was estimated as $\sim 150 \text{ M}^{-1} \text{ cm}^{-1}$, and the band was assigned as the lowest allowed $\pi\pi^*$ transition of the phenoxyl radical.³⁵ The absorption spectrum of the phenoxyl radical estimated from our global analysis of the transient absorption data (Figure 8a) also suggests this weak absorption band, which can be seen as a very long tail to the phenoxyl radical band extending from 420 nm to at least 500 nm.

It is found from the global analysis that we cannot use identical SADS for the S_1 and S_1' states and get a satisfactory fit. Nevertheless, the spectra estimated for the S_1 and S_1' states have very similar character (see Figure 8a) because they arise from the same electronic state. Both spectra have a broad ESA absorption across the UV–vis region, with a pronounced negative SE component centered around 340 nm. The small differences between the spectra of S_1 and S_1' likely reflect the relaxation

processes, vibrational relaxation, or solvation of the excited solute molecules in the solution. The SE component cannot be resolved from ESA because they originate from the same spectroscopic state, and both bands have similar dynamics. The SE center position for the relaxed S_1 state is 342 nm, which is very close to the steady state fluorescence emission band peak at 340 nm. However, the SE center for the unrelaxed S'_1 is red-shifted by 4 nm. The same result can also be obtained by careful examination of the early time transient absorption spectra shown in Figure 4d. The SE band center blue-shifts within the first ~ 3 ps. This dynamic spectral shifting phenomenon^{51,52} provides a direct observation of the relaxation process of the singlet excited state, and it agrees very well with the 1.2 ps S'_1 lifetime estimated from the global analysis.

This information allows us to further consider the identity of the vertically excited S'_1 . Recall that the 266 nm excitation is, in fact, to the blue side of the S_1 band of phenolate (Figure 1). Two candidates were suggested earlier for this shorter-lived singlet state: a vibrationally unrelaxed S_1 or an S_1 state prior to solvation dynamics. Both forms of incompletely relaxed species have been invoked in the literature as electron precursor in electron ejection from aromatic molecules.^{17,20,21} The Stein group proposed, after studying temperature and excitation wavelength dependence of photodetachment of naphtholate anion, that electron ejection occurs prior to solvent relaxation around the initially excited S_1 state,¹⁷ while from a photoionization study of indole, tryptophan and aniline derivatives Mialocq et al.²⁰ and Saito et al.,²¹ on the other hand, claimed that electron ejection results from a vibrationally unrelaxed S_1 state.

The SADS for S_1 and S'_1 in Figure 8a shows that the width of the SE band does not change noticeably during the evolution $S'_1 \rightarrow S_1$, which might provide one way to distinguish solvation dynamics from vibrational relaxation. However, the dynamic blue shift of the center position seems to exclude the solvation relaxation because the solvation would induce a red spectral shift.^{51,53} Ab initio calculations²⁶ indicate that phenolate ground state and lowest singlet excited state have very similar dipole moments, and consequently, the solvent relaxation should not be pronounced or lead to an extensive Stokes shift, as observed experimentally.^{25,54} More recent calculations by Granucci and Hynes confirm this is, indeed, the case for the 1L_b excited state,⁷ although their gas phase calculations place this state slightly higher than 1L_a . The expectation of a small solvation shift therefore provides additional evidence against attributing the difference in S'_1 and S_1 propensity in ejecting electrons to incomplete solvent relaxation.

Further, the solvated electron buildup time obtained from transient absorption for aqueous phenolate, phenol,²⁹ and β -naphtholate⁵⁵ ranges from several picoseconds to hundreds of picoseconds. Since the solvation time scale for the S_1 state is mainly determined by the nature of the solvent, with a typical time scale of a few picoseconds in water at modest solute concentrations and ionic strengths, it seems unlikely that an unsolvated singlet state is responsible for ejecting fast electrons. On the other hand, vibrational relaxation would be expected to vary considerably with the solute identity and hydrogen bonding geometries of the different solutes with water.^{51,52,56} On the basis of the above considerations, we conclude that a vibrationally hot singlet state is the precursor of the fast electron.

We see from Table 1 that the S'_1 relaxation rate k_{relax} is $3.6 \times$ the electron ejection rate k'_e . This means that most S'_1 states relax into S_1 , and only 22% detach to yield solvated electrons and phenoxyl radicals. For aromatic molecules, usually the vibrationally excited

state S'_1 relaxes quickly to the vibrational ground S_1 state, from which fluorescence is emitted.⁵⁷ This is consistent with the observation that excitation at different wavelengths across S_1 makes little difference to the shape of the emission spectrum. Results from further TCSPC measurements (not shown) indicating that the fluorescence lifetimes do not vary much with photoexcitation wavelength across the S_1 band also supports the argument for fast relaxation of S'_1 . Vibrational relaxation therefore dominates the early time decay dynamics of the photoexcited system.

Two electron ejection channels are identified in our study: a faster one competing with the relaxation process of the vertically prepared singlet state S'_1 and a slower one competing with the regular deactivation processes of the fluorescing singlet state S_1 . The slow ejection channel from the relaxed S_1 state actually contributes a larger portion of the detached electrons: 64% is contributed by S_1 and 36% by S'_1 , even though the electron ejection rate from the unrelaxed S'_1 is 6 times faster than that from the relaxed S_1 . This analysis also predicts a higher electron yield at short excitation wavelength in the S_1 absorption band: at the blue end of the band, such as 266 nm, an extra electron ejection channel opens up, and as a result, the electron production is increased. We would expect that at the red end of the S_1 absorption band (~ 310 nm) fewer electrons would be produced because only the slow ejection channel would be operative. It clearly indicates that the electron yield is not directly determined by the electron ejection rate, but rather, by the branching of competing photoinduced processes.

One of the principal results of our analysis is the demonstration that the electron ejection process from phenolate is out-competed by other excited state relaxation processes and is certainly slower compared to small inorganic molecules, such as aqueous I^- ,^{39,58} $Fe(CN)_6^{4-}$,⁵⁹ OH^- ,⁴⁴ NCS^- ,⁶⁰ and H_2O itself^{41,61,62} as well as Na^- in ethers.^{28,63} See refs 58, 62 and, 64 for reviews. For example, from ultrafast studies of these small inorganic molecules in water, it is found that the electron ejection process is fully complete within the first 1 ps, and the mechanism either involves adiabatic solvent rearrangement from a CTTS state to the solvated electron or involves directly or indirectly the water conduction band.

Deactivation of the Singlet State and the Role of the Triplet. One of the prevailing mechanisms proposed for electron photodetachment from aromatic molecules in the previous literature involves the triplet state as precursor. The triplet has significant quantum yield for photoexcited phenolic compounds and tyrosyl peptides, and Bent et al. used the idea of electron ejection from triplet state via a biphotonic process to explain photoionization of such molecules.¹⁵ Clancy and Forbes also claimed involvement of the triplet state for deprotonated tyrosine electron photodetachment in their chemically induced dynamic electron polarization (CIDEP) study.²² Meanwhile, Krauss et al.²⁶ argued that the electron is ejected via autodetachment from the phenolate triplet state, which energetically lies above the phenoxyl radical/electron pair and used it to justify the absence of the phenolate triplet transient absorption at 20 ns.¹⁵ Other efforts to look for triplet state involvement in phenolate electron detachment by means of time-resolved ESR measurement failed to support the idea above of the triplet state electron precursor but, rather, favored a singlet excited state origin of the solvated electron.^{24,25,65} Due to the short lifetimes observed for the precursor states and the excellent match with the fluorescence lifetime, our experiment cleanly establishes the precursor as a singlet but does not completely rule out some role for the triplet.

A related result emerging from this work is the unusually short intrinsic lifetime of phenolate S_1 state. Both the TCSPC and the transient absorption measurement give a consistently short lifetime of ~ 20 ps. It should be pointed out that according to the results from the global analysis, electron detachment is not the only reason for the shortened S_1 lifetime of phenolate. Without the electron ejection channel, phenolate would have an only slightly longer lifetime of 37 ps, which is still short for a simple substituted benzene system. By way of comparison, the phenol S_1 state lifetime reported in the literature is 2.1 ns in water;¹⁵ TCSPC measurements in our lab give a slightly longer fluorescence lifetime of 3.3 ns for this system.⁶⁶ The fluorescence lifetime of related molecules that undergo electron ejection in water, aniline and indole, are reported as 1.04 and 4.10 ns, respectively.^{8,21} The short S_1 lifetime for phenolate must also be due in part to the fast deactivation rate denoted by Σk . Approximately 50% of the relaxed S_1 state is dissipated through this combined Σk channel. Of the three pathways in Σk for phenolate, the radiative rate, k_r , is a small contribution because the fluorescence quantum yield, ϕ_f , is very small, estimated as 0.01 for phenolate at 266 nm at room temperature.⁶ This indicates that fast ISC or IC is as important a factor leading to the short fluorescence lifetime of phenolate as the detachment of electrons.

The quantum yield of the triplet state ϕ_T has never been measured at room temperature. But at 77 K, Ichino et al. recorded a triplet emission band that is much stronger than singlet fluorescence emission when frozen aqueous phenolate is excited at 280 nm.²⁵ Moreover, on the basis of ab initio calculations, Krauss et al. suggested that, compared with phenol, the ISC of phenolate is increased due to the reduced singlet–triplet splitting and similar eigenfunctions in the S_1 and T_1 states, allowing for better spin–orbit mixing. This would explain the lower fluorescence yield of phenolate and an enhanced intersystem crossing rate for phenolate.²⁶ Even though our transient spectroscopy does not appear to require assignment to a triplet absorption, we cannot exclude the possibility of triplet state production because the triplet may simply not absorb very much within our spectral window.

Preliminary steady-state emission measurements at long wavelengths suggest a weak phosphorescent band (between 400 and 460 nm) can be observed for aqueous room temperature phenolate that is particularly noticeable for 266 nm excitation. This band is enhanced in the presence of heavy metal ions, such as Cs^+ , which are known to enhance intersystem crossing rates. Time-resolved fluorescence (TCSPC) traces at 430 nm show a nanosecond lifetime component with no detectable rise; the amplitude of the long-lived emission is also influenced by cesium salts compared with sodium salts, confirming some population is rapidly reaching the triplet manifold. However, without knowing the exact values of k_{ic} and k_{isc} at room temperature, we cannot at this point make a conclusion regarding whether the IC or the ISC is the main channel contributing to Σk in Figure 6. Additional analysis of the triplet channel and comparison with the ultrafast photophysics of phenol is forthcoming from this laboratory.

5. CONCLUSION

Dispersed transient absorption is used to investigate the detailed ultrafast dynamics of phenolate electron detachment in aqueous solution. Assignment of the transient absorption to the solvated electron, the phenoxyl and singlet excited state absorption is made possible by adding KNO_3 to the solution as electron scavenger to resolve the electron from its geminate

phenoxyl radical. The global analysis of the transient absorption data sets is consistent with a simple target kinetic scheme, which agrees with the singlet excited state lifetime obtained independently via time-resolved fluorescence measurement.

Contrasting with electron ejection from inorganic molecules for which electron ejection is found to occur well within 1 ps upon photoexcitation, phenolate displays a delayed, biphasic ejection. Two channels are proposed to explain this: a fast one ($k'_e \sim 0.19$ ps⁻¹) from the vibrationally hot S'_1 state competing with the faster vibrational relaxation. The second channel is ejection from the relaxed S_1 state ($k_e \sim 0.027$ ps⁻¹) competing with internal conversion and intersystem crossing. From recent ultrafast studies, it seems that “slow” electron ejection may be a common phenomenon for photodetachment from aromatic molecules involving the two-channel mechanism from the S'_1 and S_1 states.

In some cases, one of the two channels may dominate over the other. It can be argued that, with this model, the average electron rise time relative to the fluorescence lifetime can be used as an indicator for the varying contribution of the S_1 and S'_1 states to the electron production. The 55 ps electron appearance time measured for photoexcited aqueous β -naphthol by Matsuzaki et al.⁵⁵ is small compared with its 8.9 ns fluorescence lifetime in water,¹⁵ and from this it can be asserted that the S'_1 channel dominates the photoejection. Electron ejection from excited indole in aqueous solution presents an extreme for the S'_1 electron ejection because compared with a fluorescence lifetime of 4.1 ns, electron ejection takes place within 200 fs,⁸ a time scale typical for the small inorganic molecules. In the other limit, from photoionization study of N,N,N',N' -tetramethyl-*p*-phenylenediamine (TMPD) in alcohols, the radical buildup time was found to be similar to the S_1 ESA decay time. This provides an example in which electron ejection from the relaxed S_1 state is the dominant channel.⁶⁷

The spectra of the solvated electron and the radical together with the relaxed and unrelaxed singlet excited state absorption are estimated as a result of the global analysis. It is interesting to note that the faster electron ejection channel actually produces fewer electrons, with the unrelaxed S'_1 state contributing 36% of them. The phenolate singlet lifetime is measured as ~ 20 ps. Our analysis shows that this unusually short lifetime is as much the result of fast internal conversion, intersystem crossing, or both, rather than electron detachment alone shortening the S_1 lifetime.

■ ASSOCIATED CONTENT

S Supporting Information. A derivation of the time-dependent radical population in the presence of electron scavenger. The reconstruction of the full experimental transient absorption data from the global target analysis (52 wavelengths) and tables of all fitting parameters from the global analysis. This material is available free of charge via the Internet at <http://pubs.acs.org>.

■ AUTHOR INFORMATION

Corresponding Author

*Phone: (213) 740-0461. Fax: (213) 740-3972. E-mail: stephen.bradforth@usc.edu.

Present Addresses

[†]Current address: Department of Biomedical Engineering, University of Wisconsin, Madison, WI 53706.

[‡]Current address: Department of Chemistry, University of California, Davis, One Shields Avenue, Davis, CA 95616.

ACKNOWLEDGMENT

The authors thank Tom Zhang, Anirban Roy, and Saptaparna Das for additional data collection and Tom Oliver for helpful comments on the manuscript. S.E.B. thanks Rienk van Grondelle for his kind hospitality in Amsterdam, which allowed a determination of the feasibility of this study in his lab. The experimental work was supported by the US National Science Foundation under Grants CHE-0311814 and CHE-0617060.

REFERENCES

- (1) Stein, G. Solvated Electron Formation and Hydrogen Evolution in the Photochemistry of Aqueous Solutions. In *Solvated Electron*; Hart, E. J., Ed.; American Chemical Society: Washington, D.C., 1965; p 230.
- (2) Porter, G.; Strachan, E. *J. Chem. Soc., Faraday Trans.* **1958**, *54*, 1595.
- (3) Dobson, G.; Grossweiner, L. I. *J. Chem. Soc., Faraday Trans.* **1965**, *61*, 708.
- (4) Land, E. J.; Porter, G.; Strachan, E. *J. Chem. Soc., Faraday Trans.* **1961**, *57*, 1855.
- (5) Grossweiner, L. I.; Zwicher, E. F. *J. Chem. Phys.* **1960**, *32*, 305.
- (6) Getoff, N. *Radiat. Phys. Chem.* **1989**, *34*, 711.
- (7) Tang, Y.; Suzuki, Y. I.; Shen, H.; Sekiguchi, K.; Kurahashi, N.; Nishizawa, K.; Zuo, P.; Suzuki, T. *Chem. Phys. Lett.* **2010**, *494*, 111.
- (8) Peon, J.; Hess, G. C.; Pecourt, J.-M. L.; Yuzawa, T.; Kohler, B. *J. Phys. Chem. A* **1999**, *103*, 2460.
- (9) Peon, J.; Hoerner, J. D.; Kohler, B. Near-Threshold Photoionization Dynamics of Indole in Water. In *Liquid Dynamics: Experiment, Simulation, and Theory*; Fourkas, J. T., Ed.; American Chemical Society: Washington, DC, 2002; Vol. 820; p 122.
- (10) Itoh, S.; Taki, M.; Fuku, S. *Coord. Chem. Rev.* **2000**, *198*, 3.
- (11) Larsen, D. S.; Vengris, M.; van Stokkum, I. H. M.; van der Horst, M. A.; de Weerd, F. L.; Hellingwerf, K. J.; van Grondelle, R. *Biophys. J.* **2004**, *86*, 2538.
- (12) Michaelis, L.; Schubert, M. P.; Granick, S. *J. Am. Chem. Soc.* **1939**, *61*, 1981.
- (13) Lewis, G. N.; Lipkin, D. *J. Am. Chem. Soc.* **1942**, *64*, 2801.
- (14) Linschitz, H.; Berry, M. G.; Schweitzer, D. *J. Am. Chem. Soc.* **1954**, *76*, 5833.
- (15) Bent, D. V.; Hayon, E. *J. Am. Chem. Soc.* **1975**, *97*, 2599.
- (16) Zechner, J.; Kohler, G.; Grabner, G.; Getoff, N. *Chem. Phys. Lett.* **1976**, *37*, 297.
- (17) Feitelson, J.; Stein, G. *J. Chem. Phys.* **1972**, *57*, 5378.
- (18) Cook, J. A. H.; Logan, S. R. *J. Photochem. Photobiol. A* **1974/1975**, *3*, 89.
- (19) Grabner, G.; Kohler, G.; Zechner, J.; Getoff, N. *J. Phys. Chem.* **1980**, *84*, 3000.
- (20) Mialocq, J. C.; Amouyal, E.; Bernas, A.; Grand, D. *J. Phys. Chem.* **1982**, *86*, 3173.
- (21) Saito, F.; Tobita, S.; Shizuka, H. *J. Photochem. Photobiol. A* **1997**, *106*, 119.
- (22) Clancy, C. M. R.; Forbes, M. D. E. *Photochem. Photobiol.* **1999**, *69*, 16.
- (23) Mittal, L. J.; Mittal, J. P. *J. Photochem. Photobiol. A* **1997**, *106*, 127.
- (24) Bussandri, A.; van Willigen, H. *J. Phys. Chem. A* **2001**, *105*, 4669.
- (25) Ichino, T.; Fessenden, R. W. *J. Phys. Chem. A* **2003**, *107*, 9257.
- (26) Krauss, M.; Jensen, J. O.; Hameka, H. F. *J. Phys. Chem.* **1994**, *98*, 9955.
- (27) Kloepfer, J. A.; Vilchiz, V. H.; Lenchenkov, V. A.; Bradforth, S. E. *Chem. Phys. Lett.* **1998**, *298*, 120.
- (28) Barthel, E. R.; Martini, I. B.; Schwartz, B. J. *J. Chem. Phys.* **2000**, *112*, 9433.
- (29) Mialocq, J. C.; Sutton, J.; Goujon, P. *J. Chem. Phys.* **1980**, *72*, 6338.
- (30) Kee, T. W.; Son, D. H.; Kambhampati, P.; Barbara, P. F. *J. Phys. Chem. A* **2001**, *105*, 8434.
- (31) Within a nanosecond time window, cross-recombination with radicals produced from different photochemical events nearby in the solution cannot occur. Geminate recombination in the liquid phase is an inhomogeneous kinetics diffusion problem in which the electron recombines with its neutral geminate partner under a weak mutual attractive potential. The decay dynamics of the radical/electron cannot be described by exponential kinetics.
- (32) Jailaubekov, A. E.; Bradforth, S. E. *Appl. Phys. Lett.* **2005**, *87*, 021107.
- (33) Tauber, M. J.; Mathies, R.; Chen, X.; Bradforth, S. E. *Rev. Sci. Instrum.* **2003**, *74*, 4958.
- (34) Kloepfer, J. A.; Bradforth, S. E.; Nadeau, J. *J. Phys. Chem. B* **2005**, *109*, 9996.
- (35) Radziszewski, J. G.; Gil, M.; Gorski, A.; Spanget-Larsen, J.; Waluk, J.; Mroz, B. *J. Chem. Phys.* **2001**, *115*, 9733.
- (36) Ichino, T. On the Mechanism of Unusual CIDEP. Ph.D. Dissertation, University of Notre Dame, South Bend, IN, 2002.
- (37) Feitelson, J.; Hayon, E.; Treinin, A. *J. Am. Chem. Soc.* **1973**, *95*, 1025.
- (38) Vilchiz, V. H.; Kloepfer, J. A.; Germaine, A. C.; Lenchenkov, V. A.; Bradforth, S. E. *J. Phys. Chem. A* **2001**, *105*, 1711.
- (39) Kloepfer, J. A.; Vilchiz, V. H.; Lenchenkov, V. A.; Germaine, A. C.; Bradforth, S. E. *J. Chem. Phys.* **2000**, *113*, 6288.
- (40) Kloepfer, J. A.; Vilchiz, V. H.; Lenchenkov, V. A.; Chen, X.; Bradforth, S. E. *J. Chem. Phys.* **2002**, *117*, 766.
- (41) Crowell, R. A.; Bartels, D. M. *J. Phys. Chem.* **1996**, *100*, 17940.
- (42) Anderson, N. A.; Hang, K.; Asbury, J. B.; Lian, T. *Chem. Phys. Lett.* **2000**, *329*, 386.
- (43) Birks, J. B. *Photophysics of Aromatic Molecules*; Wiley-Interscience: London, 1970.
- (44) Crowell, R. A.; Lian, R.; Shkrob, I. A.; Bartels, D. M.; Chen, X.; Bradforth, S. E. *J. Chem. Phys.* **2004**, *120*, 11712.
- (45) Goldschmidt, C.; Stein, G. *Chem. Phys. Lett.* **1970**, *6*, 299.
- (46) Holzwarth, A. R. Data Analysis in Time-Resolved Measurements. In *Biophysical Techniques in Photosynthesis*; Ames, J., Hoff, A. J., Eds.; Kluwer: Dordrecht, the Netherlands, 1996; p 75.
- (47) van Stokkum, I. H. M.; Larsen, D. S.; van Grondelle, R. *Biochim. Biophys. Acta, Bioenerg.* **2004**, *1657*, 82.
- (48) Rice, S. A. *Diffusion-Limited Reactions*; Elsevier: Amsterdam, 1985; Vol. 25.
- (49) Aldrich, J. E.; Bronskill, M. J.; Wolff, R. K.; Hunt, J. W. *J. Chem. Phys.* **1971**, *55*, 530.
- (50) Jortner, J. *Ber. Bunsenges. Phys. Chem.* **1971**, *75*, 696.
- (51) Stratt, R. M.; Maroncelli, M. *J. Phys. Chem.* **1996**, *100*, 12981.
- (52) Chapman, C. F.; Maroncelli, M. *J. Phys. Chem.* **1991**, *95*, 9095.
- (53) Jimenez, R.; Fleming, G. R.; Kumar, P. V.; Maroncelli, M. *Nature* **1994**, *369*, 471.
- (54) Becker, R. S. *Handbook of Fluorescent Spectra of Aromatic Molecules*; Academic Press: New York, 1969.
- (55) Matsuzaki, A.; Kobayashi, T.; Nagakura, S. *J. Phys. Chem.* **1978**, *82*, 1201.
- (56) Deák, J. C.; Iwaki, L. K.; Dlott, D. D. *J. Phys. Chem. A* **1998**, *102*, 8193.
- (57) Wawilov, W. Z. *Phys.* **1924**, *22*, 266.
- (58) Chen, X.; Bradforth, S. E. *Annu. Rev. Phys. Chem.* **2008**, *59*, 203.
- (59) Lenchenkov, V. A.; Kloepfer, J. A.; Vilchiz, V. H.; Bradforth, S. E. *Chem. Phys. Lett.* **2001**, *342*, 277.
- (60) Lian, R.; Oulianov, D.; Crowell, R. A.; Shkrob, I. A.; Chen, X.; Bradforth, S. E. *J. Phys. Chem. A* **2006**, *110*, 9071.
- (61) Elles, C. G.; Jailaubekov, A. E.; Crowell, R. A.; Bradforth, S. E. *J. Chem. Phys.* **2006**, *125*, 044515.
- (62) Elles, C. G.; Bradforth, S. E., in preparation, 2011.
- (63) Wang, Z. H.; Shoshana, O.; Hou, B. X.; Ruhman, S. *J. Phys. Chem. A* **2003**, *107*, 3009.

(64) Kloepfer, J. A.; Vilchiz, V. H.; Lenchenkov, V. A.; Bradforth, S. E. Electron photodetachment in solution. In *Liquid Dynamics: Experiment, Simulation, and Theory*; Fourkas, J., Ed.; ACS: Washington, D.C., 2002; Vol. 820; pp 108.

(65) Jeevarajan, A. S.; Fessenden, R. W. *J. Phys. Chem.* **1992**, *96*, 1520.

(66) Zhang, Y.; Roy, A.; Das, S.; Oliver, T. A. A.; Ashfold, M. N. R.; Bradforth, S. E. 2011, in preparation.

(67) Hirata, Y.; Mataga, N. *J. Phys. Chem.* **1983**, *87*, 3190.